Advanced Mathematical Models & Applications
Vol.10, No.3, 2025, pp.687-709
https://doi.org/10.62476/amma.103687

Jomard Publishing

BURGERS' EQUATION RESOLUTION USING A NEW FORMULATION OF NODAL INTEGRAL METHOD

Meryem Chahir[1*], **Najib Guessous**[1], **Souhli Hicham Amrani**[2]

[1]ENS, Sidi Mohamed Ben Abdellah University, Fez, Morocco
[2]ENSA, Chouaib Doukkali University, El Jadida, Morocco

Abstract. In the numerical approximation of physical problems, achieving a high level of accuracy is often essential. Various numerical methods have been developed to meet this requirement, including the Nodal Integral Method (NIM), which is known for delivering accurate results even on coarse meshes. In the present work, we develop a new scheme inspired by the classical NIM to solve the one-dimensional (1D) Burgers' equation. To assess the performance of the proposed approach, several numerical tests are carried out. The results clearly demonstrate the effectiveness and accuracy of the developed scheme.

Keywords: Burgers' equation, Nodal Integral Method, Modified Nodal Integral Method.
AMS Subject Classification: 35Q35, 65M06, 65M12, 76M20.
Corresponding author: Meryem, Chahir, ENS, Sidi Mohamed Ben Abdellah University, No.69, Lotissement Issam, Fez, Morocco, e-mail: *meryem.chahir@usmba.ac.ma*
Received: 6 May 2025; Revised: 27 July 2025; Accepted: 28 August 2025; Published: 3 December 2025.

1 Introduction

With the advancement of computational power, researchers are increasingly interested in solving complex mathematical problems to gain a better understanding of a wide range of physical phenomena.

The precise mathematical modeling of any physical phenomenon is a necessary step in writing the equation to be solved for the numerical simulation.

After mathematical modeling, the solutions of the partial differential equation (PDE) are approached numerically by numerical methods such as finite difference (FDM), finite element (FEM), or finite volume (FVM) methods.

For relatively complex PDEs, traditional numerical methods can be computationally expensive in terms of both processing time and memory usage. This has motivated the development of nodal methods, which enable accurate calculations on coarse meshes, making them more competitive than the other numerical methods mentioned above. To address these challenges and ensure reliable results, it is often necessary to adapt alternative coarse mesh methods (Azmy & Dorning, 1983; Lawrence, 1986; Hennart, 1986; Dorning, 1979; Steinke, 1973; Guessous, 1993; Akhmouch & Guessous, 2003; Guessous, 2003; Amrani et al., 2006).

Nodal methods were initially developed in the 1970s to solve neutron scattering equations by Burns, Dorning, Lawrence, and their collaborators in the United States (Burns, 1979; Dorning, 1979; Lawrence, 1979; Lawrence & Dorning, 1978), as well as by Wagner and Finnemann and their collaborators in Germany (Finnemann et al., 1977; Fischer & Finnemann, 1981).

Nodal methods are presented as discretization methods. Examples include the work of Azmy and Dorning (Azmy, 1982; Azmy & Dorning, 1983), specifically in the study of stationary

flows of incompressible fluids, and the work of Hennart (Hennart, 1986, 1988) who presented high-order analytical mathematical nodal and polynomial methods as non-conforming FEM, and proposed a more adequate extended analytical formalism, after critically examining the existing analytical methods, this formalism consists in integrating transversely, by Transverse Integration Process (TIP), the original PDE on all the variables minus one, which leads to sets 1D equations which are then solved "analytically" within individual cells. These localized analytical solutions accurately reflect the underlying physics of the governing equations, enabling the NIM to produce precise and efficient results even on coarse computational grids. Recent developments and applications of NIM across various problem settings are well documented in the literature (Wang & Rizwan-Uddin, 2003; Kumar et al., 2013a,b; Wang & Rizwan-Uddin, 2018; Jarrah & Rizwan-Uddin, 2021, 2022; Ahmed et al., 2024; Zhou et al., 2016; Wang et al., 2010; Gander & Kumar, 2024; Kumar et al., 2022; Jarrah & Rizwan-Uddin, 2024).

The nodal methods share with the finite difference methods (FDM) the fact that the final algebraic system has a sparse and well-structured matrix on regular meshes, but requires less grid points for the same level of precision than that provided by FDM (Lawrence, 1986; Azmy, 1985), and consequently, the size of the matrix is reduced, which leads to a faster convergence of computation.

Despite these advantages, nodal integral method (NIM) did not find full approval for solving fluid flow problems, due to a lack of efficient nonlinear solvers. This led to the development of improved versions, such as the modified nodal integral method (MNIM) and the cell-centered nodal integral method (CCNIM). The MNIM was processed and tested in the 1996s by Rizwan-Uddin using Burgers' equation (Rizwan-uddin, 1997). MNIM effectively suppresses the parasitic oscillations that affect other schemes, allows for larger time steps without convergence issues, and offers significant advantages in stability, precision, and efficiency compared to conventional finite element methods when the problem is accurately modeled in Cartesian coordinates.

The CCNIM has recently been developed to solve fluid flow problems (Raj et al., 2022; Ahmed et al., 2021, 2023; Ahmed and Singh, 2024; Ahmed et al., 2025a,b). Shober et al. (1977) were among the first to apply similar approaches to neutron diffusion equations. CCNIM builds upon the initial step of the TIP used in the conventional NIM, transforming partial differential equations into a system of ordinary differential equations (ODEs). This method has been successfully applied to a range of classical problems, including the diffusion equation, convection-diffusion equation, Burgers' equation, and the Navier–Stokes equations.

Burgers' equation is a partial differential equation introduced by Bateman in 1915 and later analyzed by Burgers in 1948. The equation is used as a model in many fields such as acoustics, continuous stochastic processes, dispersive water, shock waves, heat conduction, fluid mechanics, and turbulence (Moussa & Abd Al-Halim, 2022; Burgers, 1939).

Several schemes exist for solving the one-dimensional Burgers' equation, with the traditional NIM and the MNIM among the most well-known (Rizwan-uddin, 1997; Kumar et al., 2019a,b).

In this work, we proposed a new formulation of NIM for solving the 1D time-dependent Burgers' equation.

The novelty of the proposed scheme lies in its integral nodal formulation, which simultaneously discretizes both spatial and temporal domains within a unified framework. This approach enhances stability and accuracy in solving nonlinear convection-diffusion equations such as the Burgers' equation, outperforming traditional finite difference and finite element methods. Unlike classical NIM formulations, which determine pseudo-source terms using two constraint equations: the balance equation and the commutation condition $\bar{u}^{xt} = \bar{u}^{tx}$. The present scheme derives these terms through direct integration of the governing equations. The balance equation is then used to compute the cell-centered velocity $\bar{u}^{xt}_{i,j}$. The integral structure of the method enables a more natural treatment of boundary conditions and nonlinear terms, effectively suppressing the numerical oscillations that commonly occur in classical schemes.

Furthermore, the general structure of the proposed formulation makes it a promising candi-

date for extension to more complex fluid dynamics problems, including multidimensional flows and turbulence modeling.

The paper is organized as follows. A new scheme is proposed and evaluated through two numerical test cases to assess its efficiency. The results demonstrate that the proposed scheme provides accurate approximations.

2 Steps for solving PDEs by NIM

To solve PDEs by NIM, we must follow the steps grouped in the following diagram.

The steps required to apply NIM are outlined in Fig. 1, while Figs. 2–5 illustrate the local and global coordinate systems, as well as the averaged quantities and interface conditions involved in the formulation.

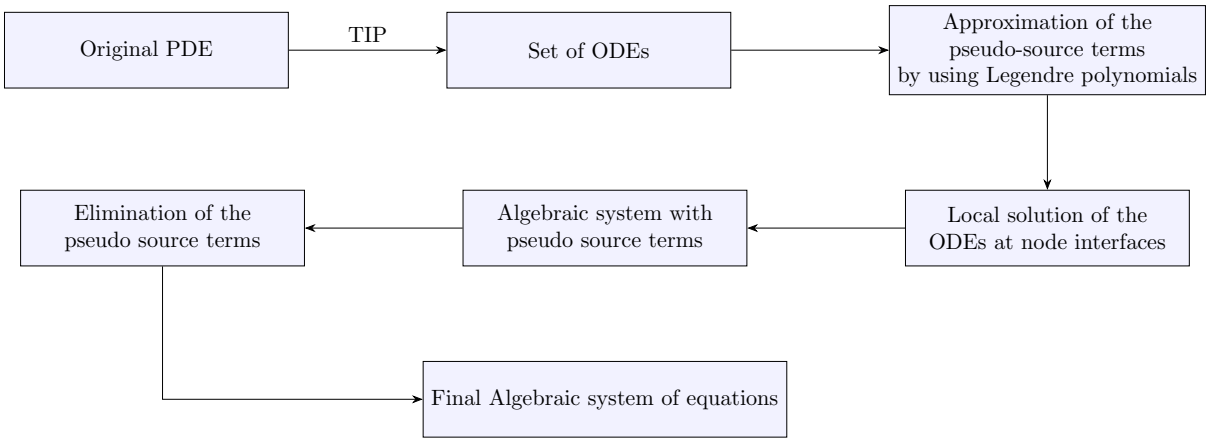

Figure 1: Flowchart of the main steps of the NIM for solving PDEs.

The flowchart illustrates the main steps of the NIM, a numerical technique designed to solve PDEs on coarse, structured meshes. The procedure begins with the TIP, in which the PDE is integrated over all independent variables except one, within a single computational node. This integration transforms the original PDE into a set of ODEs. The TIP is repeated for each spatial variable, resulting in transversely integrated ODEs that retain the dominant physical behavior of the system in reduced dimensions.

These ODEs often include complex right-hand-side terms that arise from neglected dimensions. Some of these terms are treated as known quantities and referred to as pseudo-source terms; they typically include nonlinear or inhomogeneous components of the original PDE. To make the equations tractable, these pseudo-source terms are approximated by projecting them onto a Legendre polynomial basis, then truncated to a chosen order and substituted back into the ODEs.

With these approximations in place, the ODEs are then solved analytically at the interfaces of each node, providing local solutions that depend on the unknown pseudo-source coefficients. These local interface solutions are then assembled into a global algebraic system that governs the nodal behavior.

To eliminate the pseudo-source terms from this system, two constraint equations are introduced: (i) a uniqueness condition, which ensures that the nodal average is independent of the order in which the TIP is applied, and (ii) a balance equation, obtained by integrating the original PDE over the full node volume, which establishes relationships between the pseudo-source terms across nodes.

Once these constraints are enforced, the pseudo-source terms are fully determined, yielding the final algebraic system, which can then be solved numerically using standard methods.

This analytical preprocessing, which includes transverse integration, functional approximation, and exact resolution of reduced equations, significantly improves the quality and accuracy of the solution, even when applied on coarse meshes. This feature is one of the defining strengths of nodal methods, making them particularly effective for multiscale or nonlinear problems.

Nomenclature	
Re	Reynolds number
S	Pseudo-source term
$\bar{S}^x$	Space averaged pseudo-source term
$\bar{S}^t$	Time averaged pseudo-source term
t	Total time
x	Space
$\bar{u}^x$	space averaged time dependent velocity
$\bar{u}^t$	time averaged space dependent velocity
$\bar{u}^{xt}$	centered-averaged velocity
(X, T)	Local coordinates
(x, t)	Global coordinates
τ	Temporal coordinate at a node interface
a	Spatial coordinate at a node interfacial boundary
$\bar{F}^t(x)$	The current average over t
Superscripts and subscripts	
x	Transverse integration in space
t	Transverse integration in time
i	Node index in x direction
j	Node index in t direction
Abbreviations	
NIM	Nodal Integral Method
TIP	Transverse Integration Process
MNIM	Modified–Nodal Integral Method
M2NIM	Modified–Modified–Nodal Integral Method
PDE	Partial Differential Equation
ODE	Ordinary Differential Equation
RMS	Root-Mean-Square
FDM	Finite difference method
FEM	Finite element method
FVM	Finite volume methode
NANIM	Node Averaged Nodal Integral Mehod
TIP	Transverse Integration Process

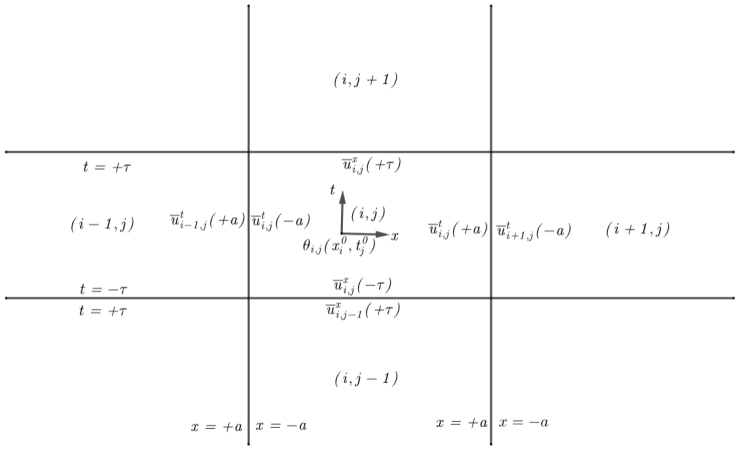

Figure 2: Local coordinate system for transverse integration of the node (i, j)

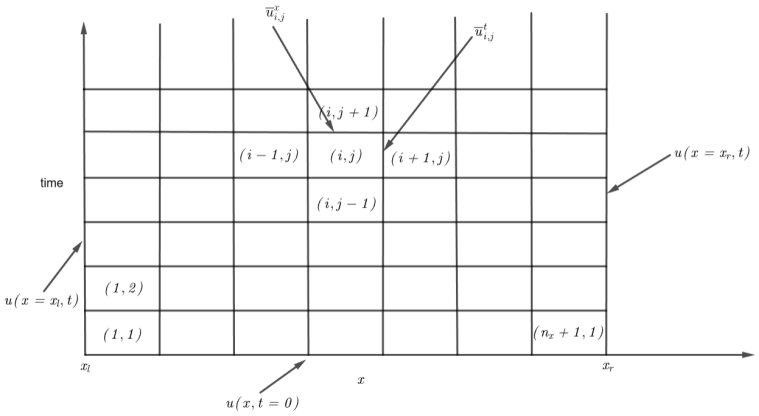

Figure 3: Schematic diagram of the global (x, t) space, and its division into computational nodes

3 Development of the scheme

Burgers' equation is one of the simplest combining both non-linear propagation And diffusive effects. The resolution of this equation attracts many mathematicians. Thus, this equation appears to be a very convenient and useful test problem For our new numerical scheme. 1D Burgers' equation is given by,

$$\begin{cases} -\dfrac{1}{Re}\dfrac{\partial^2 u(x,t)}{\partial x^2} + u(x,t)\dfrac{\partial u(x,t)}{\partial x} + \dfrac{\partial u(x,t)}{\partial t} = f(x,t) & \text{in} \quad (x_l, x_r) \times (0,T) \\ u(x_l,t) = u(x_r,t) = 0 & \text{on} \quad (0,T) \\ u(x,0) = g(x) & \text{in} \quad (x_l, x_r) \end{cases} \tag{1}$$

Here, $u(x,t)$ represents the velocity field, Re is the Reynolds number, t is time, x is the spatial variable, $x_l, x_r \in \mathbb{R}$, with $x_l < x_r$, $T > 0$, f the source term and g denotes a given set of initial data (see Figs. 3 and 4).

The temporal domain $(0,T)$ is discretized into n_t nodes indexed by subscript j, and the spatial domain (x_l, x_r) into n_x nodes indexed by i. Each space-time node has dimensions of $2a_{i,j}$ in width and $2\tau_{i,j}$ in height (see Fig. 2).

Transverse integrating the Burgers' equation over the node (i, j) over each one of the independent variables x and t. Operating equation (1) by the operator $\frac{1}{2a_{i,j}} \int_{-a_{i,j}}^{a_{i,j}} dx$, we obtain the

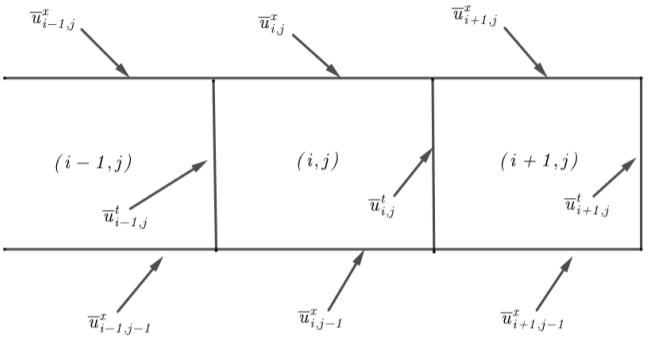

Figure 4: Averaged quantities on surfaces

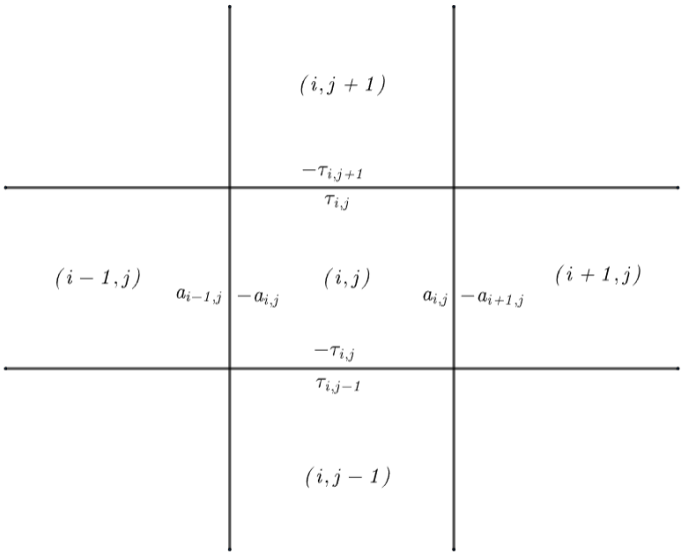

$$\bar{u}^t_{i+1,j}(-a_{i+1,j}) = \bar{u}^t_{i,j}(a_{i,j})$$
$$\frac{d\bar{u}^t_{i+1,j}(-a_{i+1,j})}{dx} = \frac{d\bar{u}^t_{i,j}(a_{i,j})}{dx}$$
$$\bar{u}^x_{i,j+1}(-\tau_{i,j+1}) = \bar{u}^x_{i,j}(\tau_{i,j})$$
$$\frac{d\bar{u}^x_{i,j+1}(-\tau_{i,j+1})}{dt} = \frac{d\bar{u}^{tx}_{i,j}(\tau_{i,j})}{dx}$$

Figure 5: The boundary conditions

space-averaged time-dependent equation,

$$\frac{d\bar{u}^x(t)}{dt} = \bar{S}^x(t) \tag{2}$$

with,

$$\begin{aligned} \bar{u}^x(t) &= \frac{1}{2a_{i,j}} \int_{-a_{i,j}}^{a_{i,j}} u(x,t)dx, \quad \text{and} \quad \bar{S}^x(t) = \\ &= \frac{1}{2a_{i,j}} \int_{-a_{i,j}}^{a_{i,j}} \left[\frac{1}{Re} \frac{\partial^2 u(x,t)}{\partial x^2} - u(x,t) \frac{\partial u(x,t)}{\partial x} + f(x,t) \right] dx \end{aligned} \tag{3}$$

$\overline{u}^x(t)$ denotes the velocity averaged over space but varying in time.

Equation (2) is obtained by integrating the original Burgers' equation over the node (i,j) with respect to the variable x. This spatial integration removes the x-dependence and results in an ODE in time for the space averaged but time dependent velocity $\bar{u}^x(t)$. More specifically, equation (2) represents the space-averaged form of the Burgers' equation, where the left-hand side denotes the time derivative of the space velocity but time dependent velocity $\bar{u}^x(t)$, and the right-hand side corresponds to the spatially averaged source term $\bar{S}^x(t)$.

Equation (3) explicitly defines the space-averaged velocity, $\bar{u}^x(t)$, and the corresponding averaged source term, $\bar{S}^x(t)$. The term $\bar{u}^x(t)$ captures the mean behavior of $u(x,t)$ over the spatial domain, while $\bar{S}^x(t)$ contains contributions from diffusion, convection, and the external source $f(x,t)$.

Realizing that the non-linear convection term will become a part of the pseudo-source term.

Then we integrate the same equation by the operator $\frac{1}{2\tau_{i,j}}\int_{-\tau_{i,j}}^{\tau_{i,j}} dt$, we obtain the next time-averaged space-dependent equation,

$$\frac{1}{Re}\frac{d^2\bar{u}^t(x)}{dx^2} = \bar{S}^t(x) \tag{4}$$

with,

$$\bar{u}^t(x) = \frac{1}{2\tau_{i,j}}\int_{-\tau_{i,j}}^{\tau_{i,j}} u(x,t)dt, \quad \text{and} \quad \bar{S}^t(x) = \frac{1}{2\tau_{i,j}}\int_{-\tau_{i,j}}^{\tau_{i,j}} \left[u(x,t)\frac{\partial u(x,t)}{\partial x} + \frac{\partial u(x,t)}{\partial t} - f(x,t)\right] dt \tag{5}$$

$\overline{u}^t(x)$ denotes the velocity averaged over time but varying in space. Equation (4) corresponds to the temporally averaged version of the original PDE, where the time variable has been eliminated. The resulting formulation depends only on the spatial coordinate x, with the second derivative of the time-averaged space dependent velocity $\bar{u}^t(x)$ balanced by the pseudo-source term $\bar{S}^t(x)$.

The treatment of Equations (4) and (2) follows the standard approach adopted in conventional NIM frameworks. In particular, the pseudo-source terms are expanded in Legendre polynomials and truncated at zeroth order, yielding constant approximations. We denote these by $\bar{S}^{tx}$ and $\bar{S}^{xt}$, corresponding to the approximations of $\bar{S}^t$ and $\bar{S}^x$, respectively. Under this assumption, integration of Equation (4) gives,

$$\frac{d\bar{u}^t(x)}{dx} = Re\bar{S}^{tx}x + C_1 = \bar{F}^t(x) \tag{6}$$

Equation (6) is obtained by performing the first integration of Equation (4) under the assumption that the pseudo-source term $\bar{S}^t(x)$ is approximated by a constant $\bar{S}^{tx}$ over the node (i,j). The resulting expression defines the first derivative of the time-averaged velocity $\bar{u}^t(x)$ with respect to the spatial variable x. The right-hand side of Equation (6) is a linear function of x, where the slope is governed by the Reynolds number Re and the constant pseudo-source term $\bar{S}^{tx}$, and C_1 is the constant of integration. This first derivative is denoted as $\bar{F}^t(x)$, which represents the spatial flux averaged over time.

The ODEs (2) and (6) can be solved analytically by direct integration. Solving Equation (6) yields,

$$\bar{u}^t(x) = Re\bar{S}^{tx}\frac{x^2}{2} + C_1x + C_2 \tag{7}$$

Similarly, integrating equation (2) provides the space-averaged time-dependent velocity $\bar{u}^x(t)$, expressed as a linear function of time,

$$\bar{u}^x(t) = \bar{S}^{xt}t + C_3 \tag{8}$$

where C_2 and C_3 are the integration constants.

To eliminate the integration constant C_1, we evaluate equation (6) at $x = a_{i,j}$, yielding

$$C_1 = \bar{F}^t(a_{i,j}) - Re\bar{S}^{tx}_{i,j}a_{i,j} \tag{9}$$

Substituting this expression for C_1 back into equation (7) and evaluating at $x = a_{i,j}$ allows us to determine the constant C_2,

$$C_2 = \bar{u}^t(a_{i,j}) - Re\bar{S}^{tx}_{i,j}\frac{a^2_{i,j}}{2} - (\bar{F}^t(a_{i,j}) - Re\bar{S}^{tx}_{i,j}a_{i,j})a_{i,j} \tag{10}$$

After substituting the expression of C_2 from equation (3) into equation (7), the time-averaged velocity $\bar{u}^t(x)$ can be rewritten as

$$\bar{u}^t(x) = \bar{u}^t(a_{i,j}) + \frac{1}{2}Re\bar{S}^{tx}_{i,j}(x - a_{i,j})^2 + \bar{F}^t(a_{i,j})(x - a_{i,j}) \tag{11}$$

Evaluating equation (11) at the point $x = -a_{i,j}$ yields the following relation,

$$\bar{u}^t(-a_{i,j}) = \bar{u}^t(a_{i,j}) + 2Rea^2_{i,j}\bar{S}^{tx}_{i,j} - 2a_{i,j}\bar{F}^t(a_{i,j}) \tag{12}$$

Now we determine the expressions of C_1 and C_2 by evaluating Equations (6) and (7) at the point $x = -a_{i,j}$. This yields,

$$\bar{u}^t(x) = \bar{u}^t(-a_{i,j}) + \frac{1}{2}Re\bar{S}^{tx}_{i,j}(x + a_{i,j})^2 + \bar{F}^t(-a_{i,j})(x + a_{i,j}) \tag{13}$$

Substituting $x = a_{i,j}$ into equation (13) yields,

$$\bar{u}^t(a_{i,j}) = \bar{u}^t(-a_{i,j}) + 2a^2_{i,j}Re\bar{S}^{tx}_{i,j} + 2a_{i,j}\bar{F}^t(-a_{i,j}) \tag{14}$$

For the node index $i + 1$, a similar expression holds,

$$\bar{u}^t(a_{i+1,j}) = \bar{u}^t(-a_{i+1,j}) + 2a^2_{i+1,j}Re\bar{S}^{tx}_{i+1,j} + 2a_{i+1,j}\bar{F}^t(-a_{i+1,j}) \tag{15}$$

Using the continuity conditions at the interface between adjacent nodes, and recognizing that $\bar{u}^t_{i+1,j}(-a_{i+1,j}) = \bar{u}^t_{i,j}(a_{i,j})$, and $\bar{F}^t_{i+1,j}(-a_{i+1,j}) = \bar{F}^t_{i,j}(a_{i,j})$, (see Fig. 5), equation (15) can be rewritten as,

$$\bar{u}^t(a_{i+1,j}) = \bar{u}^t(a_{i,j}) + 2a^2_{i+1,j}Re\bar{S}^{tx}_{i+1,j} + 2a_{i+1,j}\bar{F}^t(a_{i,j}) \tag{16}$$

By eliminating $\bar{F}^t(a_{i,j})$ from equation (12) and substituting it into equation (16), we obtain a three-point scheme relating $\bar{u}^t(-a_{i,j})$, $\bar{u}^t(a_{i,j})$, and $\bar{u}^t(a_{i+1,j})$,

$$(\frac{1}{a_{i,j}})\bar{u}^t(-a_{i,j}) - (\frac{1}{a_{i,j}} + \frac{1}{a_{i+1,j}})\bar{u}^t(a_{i,j}) + (\frac{1}{a_{i+1,j}})\bar{u}^t(a_{i+1,j}) = 2Re[a_{i,j}\bar{S}^{tx}_{i,j} + a_{i+1,j}\bar{S}^{tx}_{i+1,j}] \tag{17}$$

Assuming uniform node widths, i.e., $a_{i,j} = a_{i+1,j} = a$, the scheme simplifies to,

$$\bar{u}^t(-a_{i,j}) - 2\bar{u}^t(a_{i,j}) + \bar{u}^t(a_{i+1,j}) - 2Rea^2\bar{S}^{tx}_{i,j} - 2Rea^2\bar{S}^{tx}_{i+1,j} = 0 \tag{18}$$

The expression of $\bar{u}^x(t)$ can be derived in an analogous manner as follows,

$$\bar{u}^x(t) = \bar{u}^x(-\tau_{i,j}) + \bar{S}^{xt}_{i,j}(t + \tau_{i,j}) \tag{19}$$

Evaluating equation (19) at $t = +\tau_{i,j}$ gives,

$$\bar{u}^x(\tau_{i,j}) = \bar{u}^x(-\tau_{i,j}) + 2\tau\bar{S}^{xt}_{i,j} \tag{20}$$

which relates the space-averaged solution for node (i, j) at two successive time steps.

Now we proceed to determine the expression of the two pseudo-source terms $\bar{S}^{tx}_{i,j}$ and $\bar{S}^{xt}_{i,j}$. Here starts the difference between traditional NIM and the present scheme. In classical NIM the pseudo-source terms are determined using two contraint equations, the first one is the balance equation (intergrating the equation over all the variables), and the second one by imposing that $\bar{u}^{xt} = \bar{u}^{tx}$, on the other hand. In contrast, in our scheme, the pseudo-source terms are derived by integrating equations (11) and (19). The balance equation is then utilized to obtain an expression for the cell-centered velocity $\bar{u}^{xt}_{i,j}$.

We integrate equation (11) with respect to x over the spatial node using the operator $\frac{1}{2a_{i,j}}\int_{-a_{i,j}}^{a_{i,j}} \cdot dx$, which yields the expression of the pseudo-source term $\bar{S}_{i,j}^{tx}$ as,

$$\bar{S}_{i,j}^{tx} = \frac{3}{2a^2Re}\bar{u}_{i,j}^{tx} - \frac{3}{2a^2Re}\bar{u}^t(a_{i,j}) + \frac{3}{2aRe}\bar{F}^t(a_{i,j}) \tag{21}$$

Replacing $\bar{F}^t(a_{i,j})$ by its expression from equation (12) leads to,

$$-\bar{S}_{i,j}^{tx} - \frac{3}{a^2Re}\bar{u}_{i,j}^{tx} + \frac{3}{2a^2Re}\bar{u}^t(a_{i,j}) + \frac{3}{2a^2Re}\bar{u}^t(-a_{i,j}) = 0 \tag{22}$$

Similarly, the expression of $\bar{S}_{i,j}^{xt}$ can be determined by integrating equation (19) with respect to t over the time node using the operator $\frac{1}{2\tau_{i,j}}\int_{-\tau_{i,j}}^{\tau_{i,j}} \cdot dt$, yielding, $\frac{1}{2\tau_{i,j}}\int_{-\tau_{i,j}}^{\tau_{i,j}} dt$ as,

$$\bar{S}_{i,j}^{xt} = \frac{\bar{u}_{i,j}^{xt} - \bar{u}^x(-\tau_{i,j})}{\tau_{i,j}} \tag{23}$$

To determinate the expressions of $\bar{S}_{i,j}^{xt}$ and $\bar{S}_{i,j}^{tx}$, one additional constraint equation is required. This equation is obtained by applying the operator $\frac{1}{2a_{i,j}}\frac{1}{2\tau_{i,j}}\int_{-\tau_{i,j}}^{\tau_{i,j}}\int_{-a_{i,j}}^{a_{i,j}} dx\,dt$ to equation (1)

$$\frac{1}{2a_{i,j}}\int_{-a_{i,j}}^{a_{i,j}} -\frac{1}{Re}\frac{d^2\bar{u}^t(x)}{dx^2}dx + \frac{1}{2a_{i,j}}\frac{1}{2\tau_{i,j}}\int_{-a_{i,j}}^{a_{i,j}}\int_{-\tau_{i,j}}^{\tau_{i,j}} u(x,t)\frac{\partial u(x,t)}{\partial x}dtdx + \frac{1}{2\tau_{i,j}}\int_{-\tau_{i,j}}^{\tau_{i,j}}\frac{d\bar{u}^x(t)}{dt}dt - \frac{1}{2a_{i,j}}\frac{1}{2\tau_{i,j}}\int_{-a_{i,j}}^{a_{i,j}}\int_{-\tau_{i,j}}^{\tau_{i,j}} f(x,t)dtdx = 0 \tag{24}$$

Using the definitions of the pseudo source terms given in eqs. (2) and (4), respectively, and the identity $u(x,t)\frac{\partial u(x,t)}{\partial x} = \frac{1}{2}\frac{\partial}{\partial x}\left(u^2(x,t)\right)$, we obtain the relation between $\bar{S}_{i,j}^{xt}$ and $\bar{S}_{i,j}^{tx}$ as,

$$\bar{S}_{i,j}^{tx} - \bar{S}_{i,j}^{xt} - \frac{1}{2}\overline{\frac{\partial u^2}{\partial x}}^{tx} + \bar{f}_{i,j}^{xt} = 0 \tag{25}$$

$\overline{\frac{\partial u^2}{\partial x}}^{tx}$ is approximated by $\overline{\frac{\partial(\bar{u}^t)^2}{\partial x}}^{x}$, such by $\frac{\bar{u}^t(a_{i,j})^2 - \bar{u}^t(-a_{i,j})^2}{2a}$. Substituting this approximation into eq. (25) yields the following expression,

$$\bar{S}_{i,j}^{tx} - \bar{S}_{i,j}^{xt} - \frac{1}{4a}[\bar{u}^t(a_{i,j})^2 - \bar{u}^t(-a_{i,j})^2] + \bar{f}_{i,j}^{xt} = 0 \tag{26}$$

After substituting the expressions of $\bar{S}_{i,j}^{tx}$ and $\bar{S}_{i,j}^{xt}$ given respectively in equations (22) and (23), and by imposing the fact that $\bar{u}_{i,j}^{xt} = \bar{u}_{i,j}^{tx}$, while assuming that the time step $\tau_{i,j} = \tau$ is uniform, we obtain,

$$[-\frac{3}{a^2Re} - \frac{1}{\tau}]\bar{u}_{i,j}^{xt} + \frac{3}{2a^2Re}\bar{u}^t(a_{i,j}) + \frac{3}{2a^2Re}\bar{u}^t(-a_{i,j}) + \frac{1}{\tau}\bar{u}^x(-\tau_{i,j}) - \frac{\bar{u}^t(a_{i,j})^2 - \bar{u}^t(-a_{i,j})^2}{4a} + \bar{f}_{i,j}^{xt} = 0 \tag{27}$$

The non-linear term $\frac{\bar{u}^t(a_{i,j})^2 - \bar{u}^t(-a_{i,j})^2}{4a}$ can be approximate by $\frac{(u_0)_{i,j}}{2a}(\bar{u}^t(a_{i,j}) - \bar{u}^t(-a_{i,j}))$. Thus, equation (27) can be rewritten as,

$$[-\frac{3}{a^2Re} - \frac{1}{\tau}]\bar{u}_{i,j}^{xt} + [\frac{3}{2a^2Re} - \frac{(u_0)_{i,j}}{2a}]\bar{u}^t(a_{i,j}) + [\frac{3}{2a^2Re} + \frac{(u_0)_{i,j}}{2a}]\bar{u}^t(-a_{i,j}) + \frac{1}{\tau}\bar{u}^x(-\tau_{i,j}) + \bar{f}_{i,j}^{xt} = 0 \tag{28}$$

where $(u_0)_{i,j} = \frac{\bar{u}^t(a_{i,j}) + \bar{u}^t(-a_{i,j})}{2}$ denotes the node averaged velocity at current time step.

Now we have five equations (18), (20), (22), (23) and (28), with five unknowns $\bar{u}^x$, $\bar{u}^t$, $\bar{S}^{xt}$, $\bar{S}^{tx}$, and $\bar{u}^{xt}$, we can solve this by any of the standard numerical solvers. To reduce the system to three equations, as in traditional NIM, we substitute the expressions of $\bar{S}^{tx}$ and $\bar{S}^{xt}$ from equations (22) and (23) into equations (18) and (20). This yields a set of three final algebraic equations.

4 Numerical results

To test the efficiency of the developed scheme, we consider the Burgers' equation with differences boundary conditions.

4.0.1 Test 1

To check the efficiency of the developed scheme , we consider the Burgers' equation defined by,

$$-\frac{1}{Re}\frac{\partial^2 u(x,t)}{\partial x^2} + u(x,t)\frac{\partial u(x,t)}{\partial x} + \frac{\partial u(x,t)}{\partial t} = 0 \ ; \ -2 \leq x \leq 2 \ , \ 0 \leq t \leq T$$

where, for the sake of convenience, u is subject to the boundary conditions

$$u(-2,t) = u(2,t) = 0 \quad \text{and} \quad u(x,0) = g(x) = \frac{2\pi\beta \sin(\pi x)}{Re(\alpha + \beta\cos(\pi x))}$$

The exact solution of this equation is,

$$u(x,t) = \frac{2\pi\beta \exp(\frac{-\pi^2 t}{Re}) \sin(\pi x)}{Re(\alpha + \beta \exp(\frac{-\pi^2 t}{Re}) \cos(\pi x))}$$

Figures 6–8 display the numerical results obtained using the proposed scheme, along with the corresponding exact analytical solutions of the Burgers' equation. Figure 6 presents a comparison between the exact and numerical values of the space-averaged, time-dependent velocity component $\bar{u}^x$. Figure 7 shows the exact and approximate profiles of the time-averaged, space-dependent velocity component $\bar{u}^t$, while Figure 8 illustrates the exact and numerical results for the centered-averaged velocity component $\bar{u}^{xt}$. As shown, the numerical results closely match the exact solutions, confirming the accuracy and effectiveness of the proposed scheme.

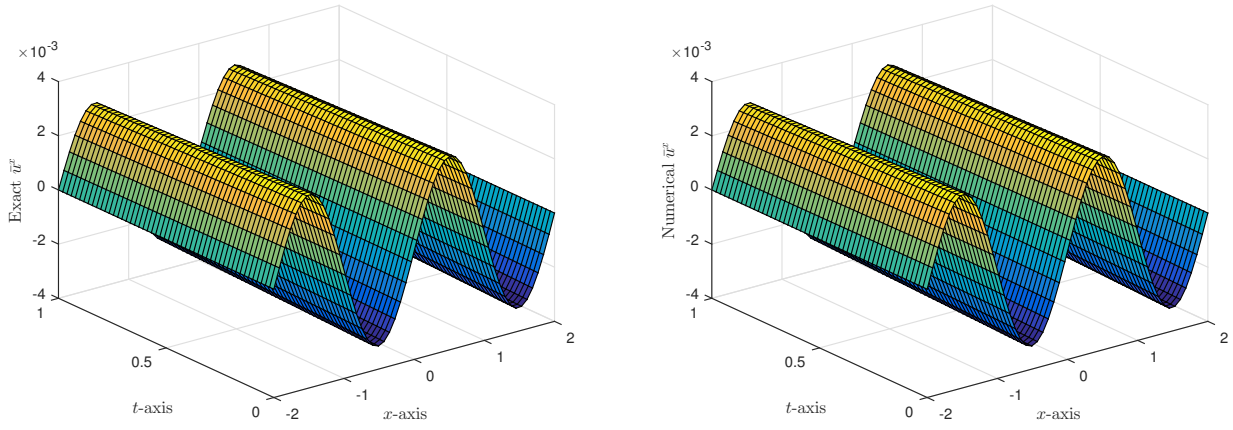

(a) **(b)**

Figure 6: Comparison between (a) the exact and (b) the numerical values of the space-averaged, time-dependent velocity component $\bar{u}^x$ at $T = 1$, $\tau = 0.02$, $\alpha = 4$, $\beta = 0.2$, $Re = 100$, and $a = 0.08$

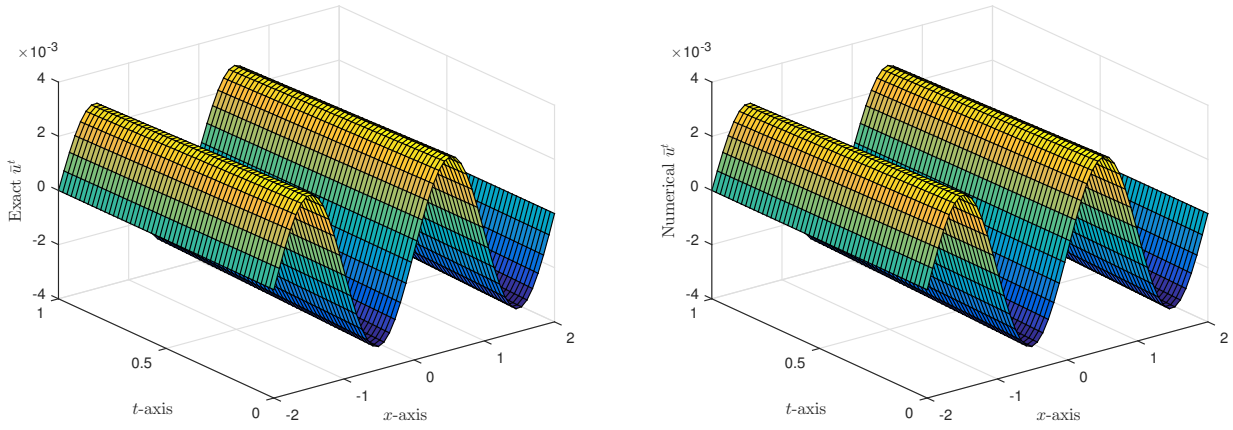

(a) **(b)**

Figure 7: Comparison between (a) the exact and (a) numerical time-averaged space-dependent velocity ($\bar{u}^t$) at $T = 1$, $\tau = 0.02$, $\alpha = 4$, $\beta = 0.2$ and $a = 0.08$

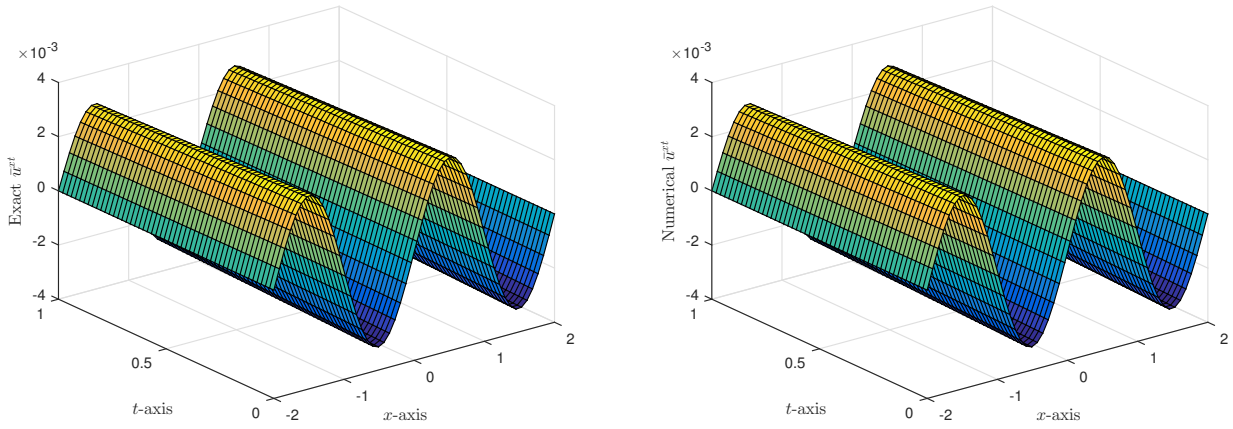

(a) **(b)**

Figure 8: Comparison between (a) the exact and (b) the numerical centered-averaged velocity ($\bar{u}^{xt}$) at $T = 1$, $\tau = 0.02$, $\alpha = 4$, $\beta = 0.2$ and $a = 0.08$

The root mean square (RMS) error, which quantifies the difference between the numerical and exact solutions, is defined as

$$RMS = \frac{1}{\sqrt{N}} \sqrt{\sum_{i=1}^{N} (\bar{u}_{i,numerical} - \bar{u}_{i,exact})^2},$$

where the RMS error is computed separately for each of the variables $\bar{u}^x$, $\bar{u}^t$, and $\bar{u}^{xt}$. In this expression, $\bar{u}_{i,\text{numerical}}$ and $\bar{u}_{i,\text{exact}}$ denote respectively the numerical and exact values of one of these velocity components.

Here N denotes the total number of discrete unknowns. For the steady-state solution shown in Figures 6 – 8, the computed RMS errors for the space-averaged velocity $\bar{u}^x$, the time-averaged velocity $\bar{u}^t$, and the centered-averaged velocity $\bar{u}^{xt}$ are 6.59×10^{-5}, 2.66×10^{-4}, and 6.67×10^{-5}, respectively. Figures 9, 10, and 11 illustrate the error for each corresponding velocity component, demonstrating the high accuracy of the proposed numerical scheme.

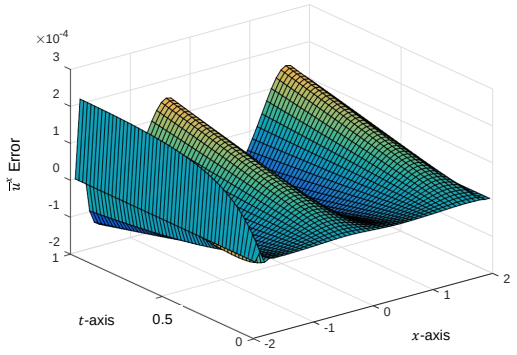

Figure 9: Error between the exact and numerical solutions of the space-averaged velocity component $\bar{u}^x$.

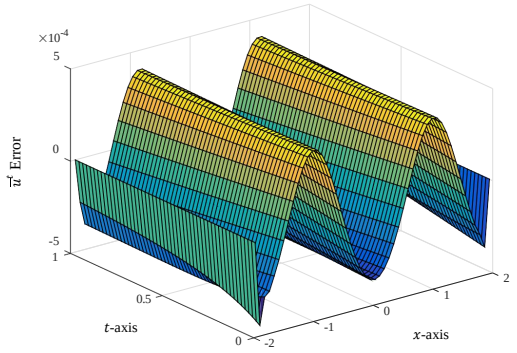

Figure 10: Error between the exact and numerical values of the time-averaged velocity component $\bar{u}^t$.

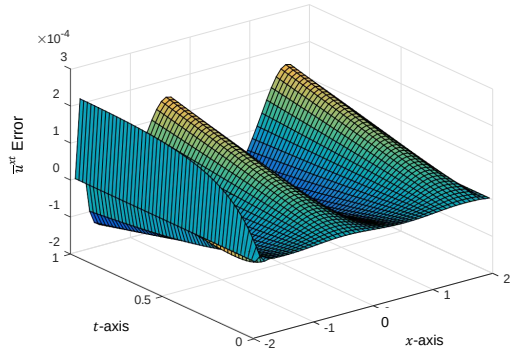

Figure 11: Error between the exact and numerical values of the centered-averaged velocity component $\bar{u}^{xt}$.

Figures 9–11 show the Errors for each averaged velocity component, confirming the high accuracy and stability of the present scheme.

4.0.2 Test 2

Now we consider the Burgers' equation defined by,

$$-\frac{1}{Re}\frac{\partial^2 u(x,t)}{\partial x^2} + u(x,t)\frac{\partial u(x,t)}{\partial x} + \frac{\partial u(x,t)}{\partial t} = f(x,t)\ ;\ -1 \le x \le 1\ ,\ 0 \le t \le T$$

with the boundary conditions

$$u(-1,t) = u(1,t) = -\frac{1}{4}\exp(\frac{-t}{Re}) \quad \text{and} \quad u(x,0) = \frac{1}{4}\cos(\pi x)$$

and the source term,

$$f(x,t) = \frac{e^{-t/Re}cos(\pi x)}{4Re}[\pi^2 - \frac{\pi Re\ e^{-t/Re}}{4}sin(\pi x) - 1]$$

The exact solution of this equation is given as,

$$u(x,t) = \frac{1}{4}\exp(\frac{-t}{Re})\cos(\pi x)$$

Figure 12 displays the comparison between the exact and the space-averaged, time-dependent velocity ($\bar{u}^x$). Similarly, Figures 13 and 14 show the comparisons for the time-averaged, space-dependent velocity ($\bar{u}^t$) and the centered-averaged velocity ($\bar{u}^{xt}$), respectively. The numerical simulations were performed with the following parameters: $T = 1$, $Re = 10$, $nx = 80$, $nt = 80$, $\tau = 0.0125$, and $a = 0.025$. The results demonstrate a close agreement with the exact solution, confirming the accuracy of the proposed scheme for this second test case with a source term.

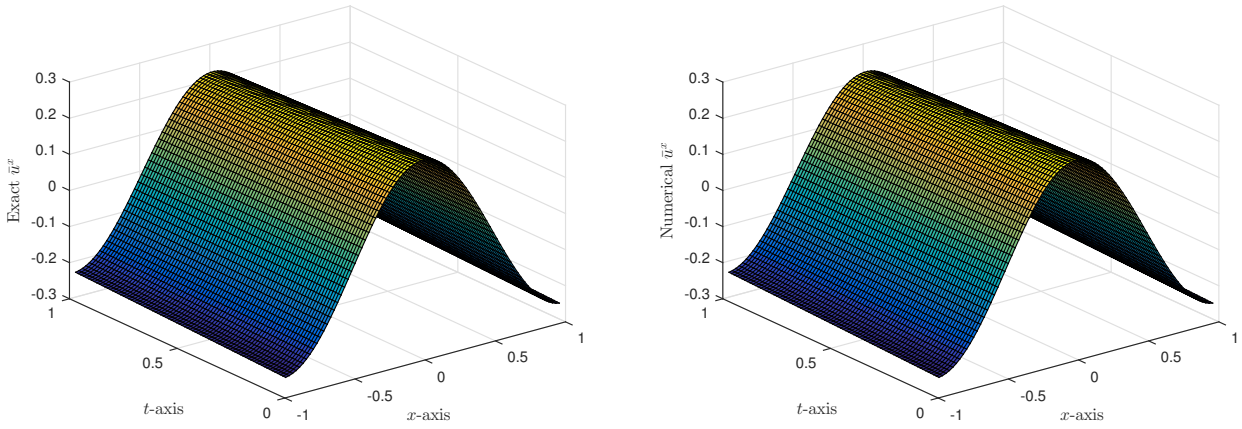

(a) **(b)**

Figure 12: Comparison between (a) the exact and (b) the numerical values of the space-averaged, time-dependent velocity component $\bar{u}^x$ for Test 2 with $T = 1$, $Re = 10$, $n_x = 80$, $n_t = 80$, $\tau = 0.0125$, and $a = 0.025$.

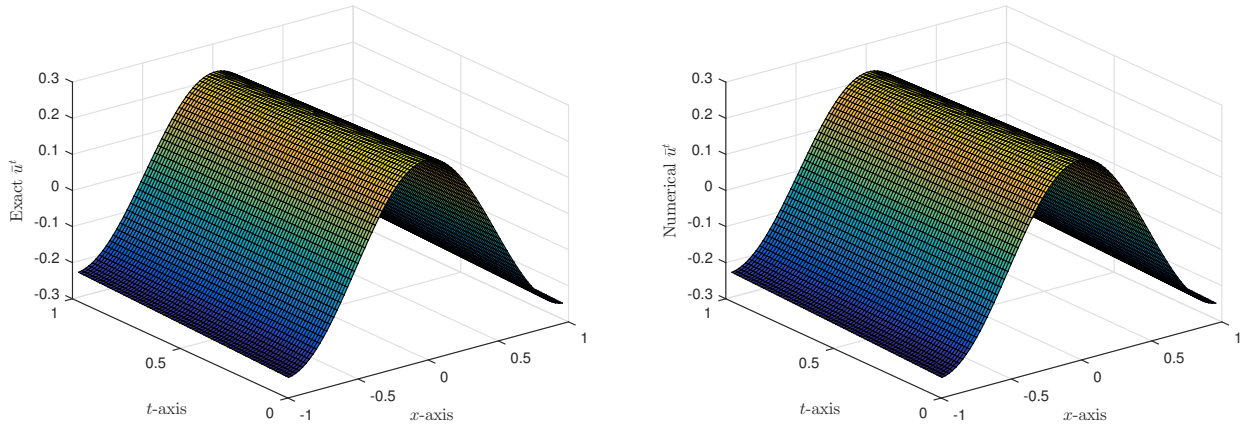

(a) **(b)**

Figure 13: Comparison between (a) the exact and (b) the numerical values of the time-averaged, space-dependent velocity component $\bar{u}^t$ for Test 2 with $T = 1$, $Re = 10$, $n_x = 80$, $n_t = 80$, $\tau = 0.0125$, and $a = 0.025$.

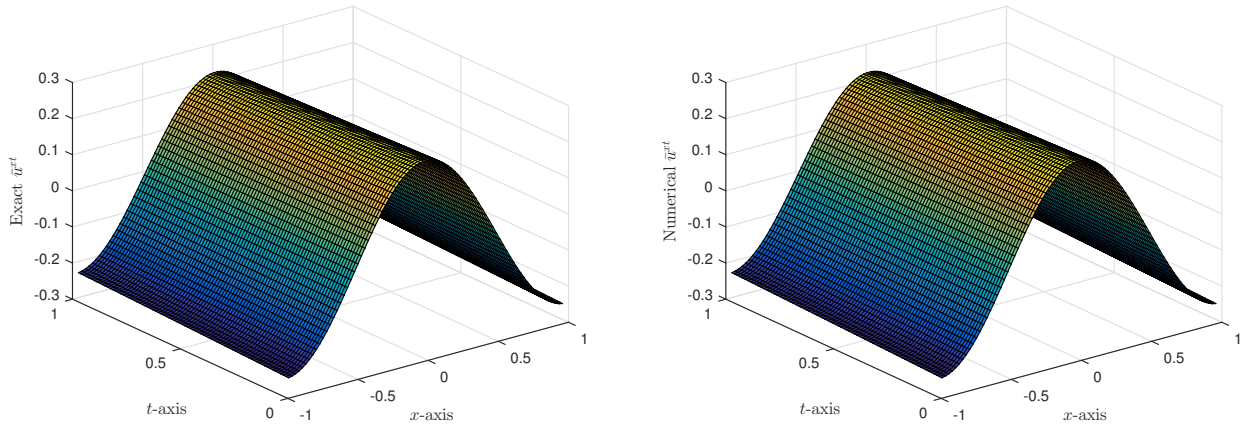

(a) **(b)**

Figure 14: Comparison between (a) the exact and (b) the numerical values of the centered-averaged velocity component $\bar{u}^{xt}$ for Test 2 with $T = 1$, $Re = 10$, $n_x = 80$, $n_t = 80$, $\tau = 0.0125$, and $a = 0.025$.

To evaluate the accuracy of the proposed scheme for Test 2, the root mean square errors between the numerical and exact solutions were calculated for each averaged velocity component. The RMS errors for $\bar{u}^x$, $\bar{u}^t$, and $\bar{u}^{xt}$ were found to be 3.29×10^{-2}, 3.29×10^{-2}, and 3.25×10^{-2}, respectively. Figures 15, 16, and 17 show the RMS error profiles for these three components. These results confirm the consistency and accuracy of the proposed scheme when applied to problems with a non-zero source term.

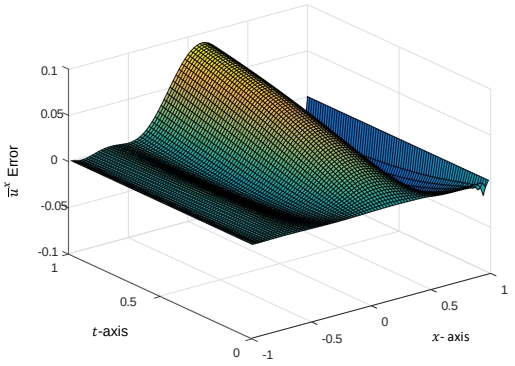

Figure 15: RMS error between the exact and numerical values of the space-averaged velocity component $\bar{u}^x$ for Test 2 with $T = 1$, $Re = 10$, $n_x = 80$, $n_t = 80$, $\tau = 0.0125$, and $a = 0.025$.

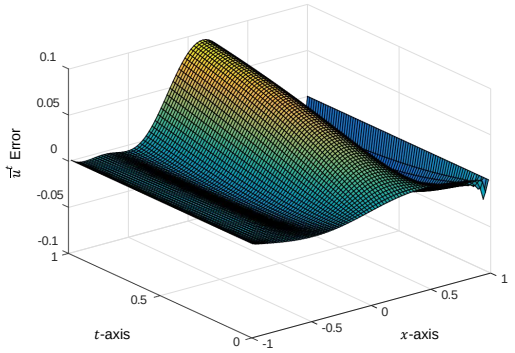

Figure 16: RMS error between the exact and numerical values of the time-averaged velocity component $\bar{u}^t$ for Test 2 with $T = 1$, $Re = 10$, $n_x = 80$, $n_t = 80$, $\tau = 0.0125$, and $a = 0.025$.

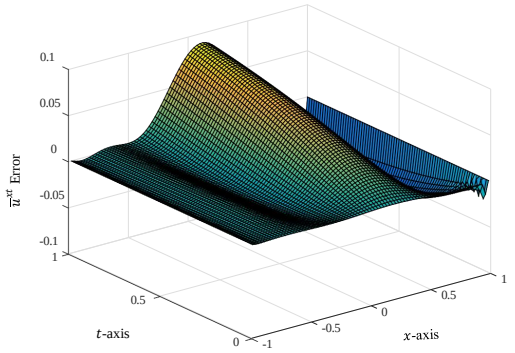

Figure 17: RMS error between the exact and numerical values of the centered-averaged velocity component $\bar{u}^{xt}$ for Test 2 with $T = 1$, $Re = 10$, $n_x = 80$, $n_t = 80$, $\tau = 0.0125$, and $a = 0.025$.

5 Discussion

To demonstrate the accuracy and the efficiency of the proposed scheme, Burgers' equation with different conditions is solved, and the numerical results are compared with the exact solution for different values of Re, n_x and n_t.

5.0.1 Test 1

To assess the performance of the proposed scheme, we consider the one-dimensional Burgers' equation solved up to the final time $T = 1$, with parameters set to $\tau = 0.0125$, $\alpha = 4$, $\beta = 0.2$, and $a = 0.05$, under Dirichlet boundary conditions. Numerical results are evaluated against the analytical solution for various Reynolds numbers. Figures 18 to 23 present side-by-side comparisons of the exact and numerical solutions for $\mathrm{Re} = 1, 10, 50, 100, 1000$, and 10000, highlighting the method's accuracy and robustness across a wide range of flow regimes.

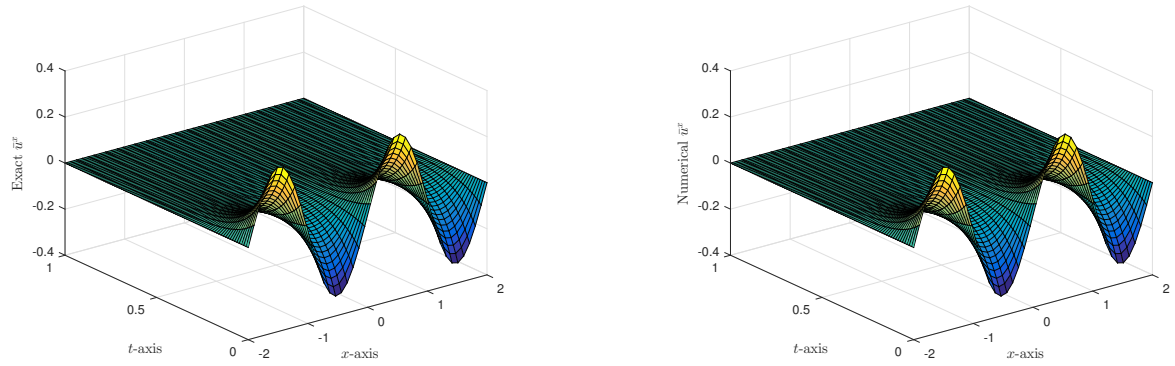

(a) Exact solution **(b)** Numerical solution

Figure 18: Comparison of exact and numerical solutions for Reynolds number $\mathrm{Re} = 1$

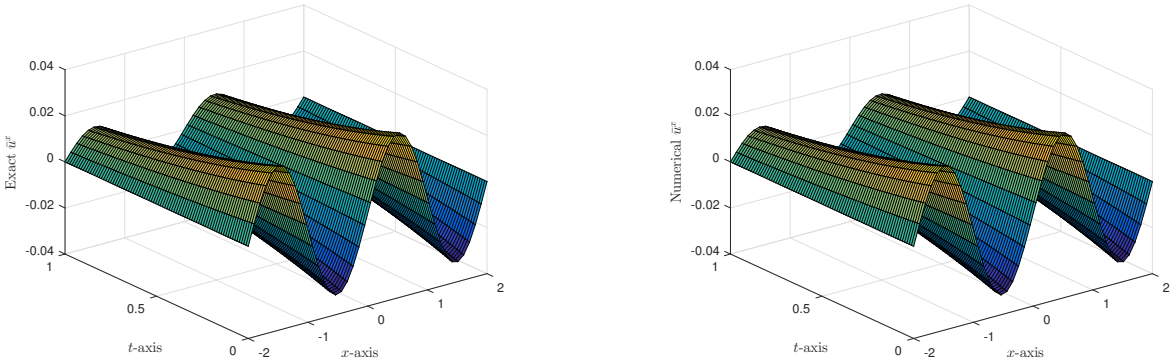

(a) Exact solution **(b)** Numerical solution

Figure 19: Comparison of exact and numerical solutions for Reynolds number $\mathrm{Re} = 10$

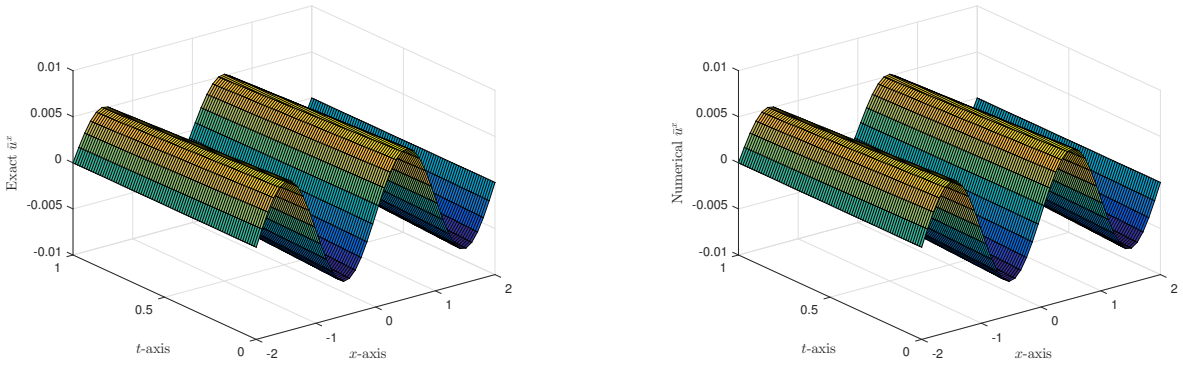

(a) Exact solution **(b)** Numerical solution

Figure 20: Comparison of exact and numerical solutions for Reynolds number Re = 50

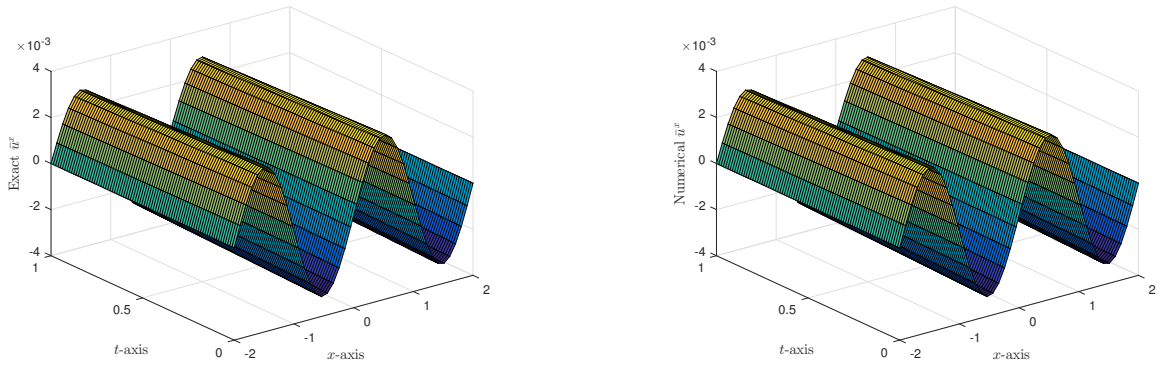

(a) Exact solution **(b)** Numerical solution

Figure 21: Comparison of exact and numerical solutions for Reynolds number Re = 100

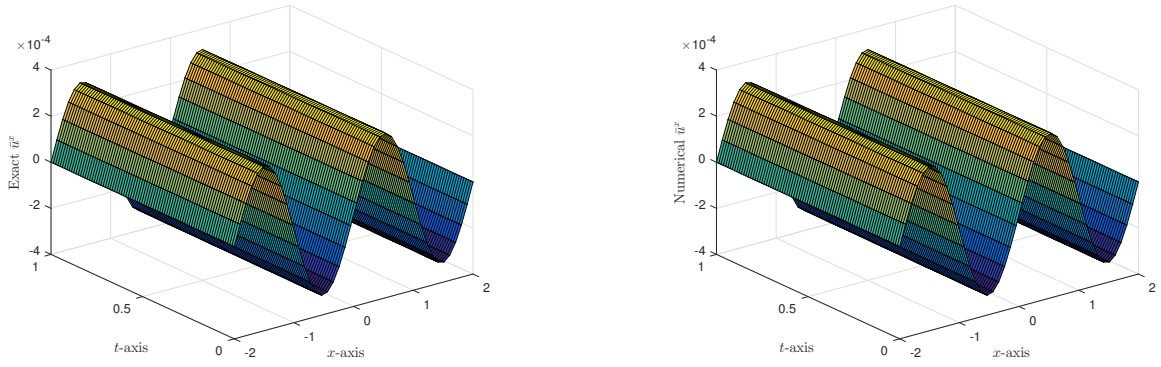

(a) Exact solution **(b)** Numerical solution

Figure 22: Comparison of exact and numerical solutions for Reynolds number Re = 1000

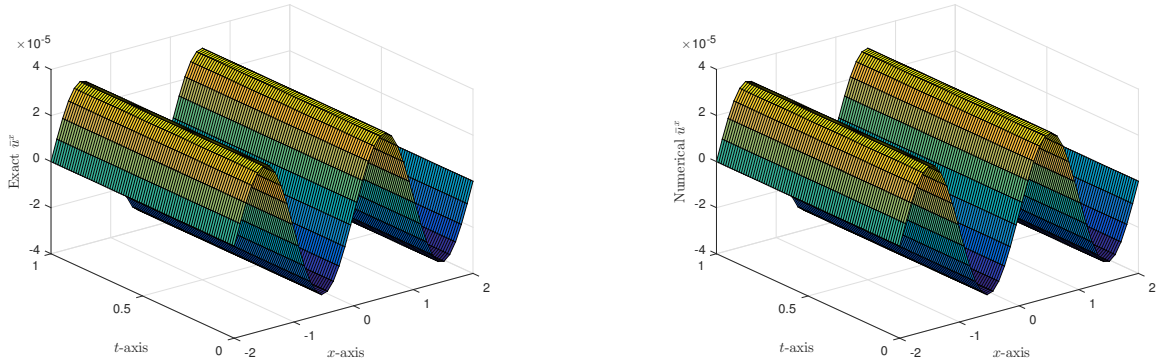

(a) Exact solution **(b)** Numerical solution

Figure 23: Comparison of exact and numerical solutions for Reynolds number Re = 10000

Figures 18 to 23 clearly demonstrate the robustness and accuracy of the proposed nodal integral formulation across a wide range of Reynolds numbers. As the Reynolds number increases from 10 to 10000, the numerical solution remains in good agreement with the analytical one. This highlights the scheme's capability to effectively capture nonlinear behavior even in convection-dominated regimes. Notably, the method maintains both stability and precision at high Reynolds numbers (Re = 1000 and Re = 10000), which are typically challenging for classical schemes. These graphical results support the effectiveness of the proposed approach for solving complex transport phenomena.

The corresponding numerical errors are summarized in Table 1.

Table 1: RMS errors of the proposed NIM scheme for the 1D Burgers' equation at varying Reynolds numbers. Parameters: $T = 1$, $n_x = 80$, $n_t = 80$, $\tau = 0.0125$, $\alpha = 4$, $\beta = 0.2$, and $a = 0.05$.

Re	$\bar{u}^x$ RMS error	$\bar{u}^t$ RMS error	$\bar{u}^{xt}$ RMS error
1	2.08836e-02	3.0996e-02	3.0682e-02
10	3.7625e-03	3.9843e-03	3.8087e-03
100	6.3232e-05	1.7365e-04	6.3748e-05
150	2.9553e-05	1.1359e-04	2.9767e-05
300	8.3208e-06	5.6522e-05	8.3609e-06
400	5.0005e-06	4.2454e-05	5.0182e-06
500	3.3891e-06	3.4013e-05	3.3975e-06
1000	1.0247e-06	1.7083e-05	1.0240e-06
5000	5.4951e-08	3.4355e-06	5.4688e-08
10000	1.4456e-08	1.7193e-06	1.4378e-08
100000	1.5186e-10	1.7207e-07	1.5094e-10

Table 1 provides a quantitative comparison, further demonstrating the reliability of the proposed approach over a wide range of Reynolds numbers. As the Reynolds number increases from 1 to 100000, the RMS errors decrease significantly, especially for the centered-averaged velocity error $\bar{u}^{xt}$, which drops from $\mathcal{O}(10^{-2})$ to $\mathcal{O}(10^{-10})$. This highlights the scheme's ability to handle nonlinearities without generating spurious oscillations. Notably, the method remains stable and accurate even at high Reynolds numbers ($Re = 10000$ and $Re = 100000$), which often pose challenges for classical methods. These results support the efficiency of the proposed method in solving convection-dominated flows.

To further assess the convergence properties of the proposed scheme, we examine the effect of varying the time step size τ on the accuracy of the numerical solution. Keeping other parameters fixed ($Re = 100$, $T = 1$, $\alpha = 4$, and $\beta = 0.2$), we compute the RMS errors for different values of τ, as shown in Table 2.

Table 2: RMS errors of the proposed NIM scheme for the 1D Burgers' equation at various time step sizes τ. Parameters used: $Re = 100$, $T = 1$, $\alpha = 4$, and $\beta = 0.2$.

Time step size τ	$\bar{u}^x$ RMS Error	$\bar{u}^t$ RMS Error	$\bar{u}^{xt}$ RMS Error
0.05	6.9926e-05	6.3454e-04	7.1029e-05
0.03	6.9862e-05	4.3080e-04	7.0807e-05
0.025	6.7729e-05	3.2777e-04	6.8566e-05
0.0125	6.3232e-05	1.7365e-04	6.3748e-05
0.01	6.2455e-05	1.4383e-04	6.2879e-05

Table 2 illustrates the effect of the time step size τ on the accuracy of the numerical solution. As τ decreases from 0.05 to 0.01, all RMS error metrics ($\bar{u}^x$, $\bar{u}^t$, and $\bar{u}^{xt}$) consistently decrease, confirming the convergence of the scheme with respect to time discretization. The relatively small reduction in spatial error $\bar{u}^x$ reflects that spatial discretization dominates in this setup, while the temporal and combined errors show more sensitivity to τ. These results demonstrate that the method maintains stability and accuracy for sufficiently small time steps.

In order to illustrate the effectiveness of the suggested approach, it is necessary to do a number of calculations on progressively fine-tuned grids. This grid refinement process allows us to observe the convergence behavior of our solution and how the accuracy improves as the mesh becomes finer (see Table 3). Table 3 presents the RMS errors for the quantities $\bar{u}^x$, $\bar{u}^t$, and $\bar{u}^{xt}$ over the specified domain with grid sizes n_x and n_t ranging from 10 to 100. A clear trend of decreasing RMS errors is observed for all three quantities as the grid sizes increase. This decreasing confirms that the numerical method demonstrates good convergence properties.

Table 3: RMS errors of the proposed formulation of NIM scheme for the 1D Burgers' equation over the domain $-2 \leq x \leq 2$, $0 \leq t \leq 1$, with parameters $\alpha = 5$, $\beta = 4$, and $Re = 10$, for varying spatial and temporal resolutions.

n_x	n_t	$\bar{u}^x$ RMS Error	$\bar{u}^t$ RMS Error	$\bar{u}^{xt}$ RMS Error
10	10	2.4147e-01	3.5550e-01	2.4807e-01
20	20	2.1538e-01	2.4017e-01	2.1550e-01
30	30	2.1123e-01	2.1518e-01	2.1097e-01
40	40	1.9435e-01	1.9452e-01	1.9435e-01
50	50	1.8248e-01	1.8205e-01	1.8261e-01
60	60	1.7531e-01	1.7482e-01	1.7547e-01
70	70	1.7092e-01	1.7049e-01	1.7108e-01
80	80	1.6809e-01	1.6774e-01	1.6825e-01
90	90	1.6618e-01	1.6589e-01	1.6633e-01
100	100	1.6483e-01	1.6458e-01	1.6497e-01

As shown in Table 3, the RMS errors decrease consistently as the grid resolution increases, confirming the expected convergence of the method. This trend holds for spatial, temporal, and combined error measures, demonstrating that the proposed new formulation of the nodal integral method accurately captures the solution behavior with mesh refinement. The results reinforce the stability and reliability of the scheme for solving the nonlinear Burgers' equation on finer grids.

5.0.2 Test 2

In order to illustrate the effectiveness of the present scheme, observe the convergence behavior of our solution, as we did with the first test, a number of calculations on progressively fine-tuned grids will be done. Table 4 presents the RMS errors for $\bar{u}^x$, $\bar{u}^t$, and $\bar{u}^{xt}$ over the specified domain with grid sizes n_x and n_t ranging from 10 to 100. A decreasing RMS errors is observed for all the above three quantities as the grid sizes increase. This decreasing confirms that the numerical method demonstrates good convergence properties.

Table 4: RMS errors of the proposed NIM scheme for the 1D Burgers' equation at $T = 1$ and $Re = 10$, for various grid sizes $n_x = n_t$.

n_x	n_t	$\bar{u}^x$ RMS Error	$\bar{u}^t$ RMS Error	$\bar{u}^{xt}$ RMS Error
10	10	3.7343e-02	6.0261e-02	3.4859e-02
20	20	3.4929e-02	4.1817e-02	3.3465e-02
30	30	3.4282e-02	3.7006e-02	3.3287e-02
40	40	3.3832e-02	3.5087e-02	3.3083e-02
50	50	3.3493e-02	3.4102e-02	3.2895e-02
60	60	3.3233e-02	3.3517e-02	3.2735e-02
70	70	3.3029e-02	3.3134e-02	3.2603e-02
80	80	3.2866e-02	3.2867e-02	3.2494e-02
90	90	3.2734e-02	3.2671e-02	3.2403e-02
100	100	3.2624e-02	3.2522e-02	3.2327e-02

As shown in Table 4, the RMS errors in space, time, and combined space-time domains exhibit a decreasing trend as the number of grid points increases. This behavior confirms the convergence of the proposed method with respect to grid refinement. The small and stable values across all error types highlight the robustness and accuracy of the scheme, even on coarser grids. These results validate the effectiveness of the present scheme and support its applicability for solving nonlinear PDEs such as the Burgers' equation. The modifications introduced in the developed scheme is motivated by the results obtained in Table 4.

Fig. 24 illustrates the comparison between the exact solution and the numerical results obtained using the proposed scheme for two different Reynolds numbers: a low Reynolds number (Re = 1) in panel (a) and a moderate Reynolds number (Re = 10) in panel (b). The primary objective here is to assess the scheme's behavior by tracking the solution's evolution at two distinct times, $T = 1$ and $T = 2$.

These results illustrate how the proposed scheme captures the evolution of the solution over time. The good agreement with the exact solution at both time instances indicates that the method is capable of reliably tracking the temporal dynamics of the solution.

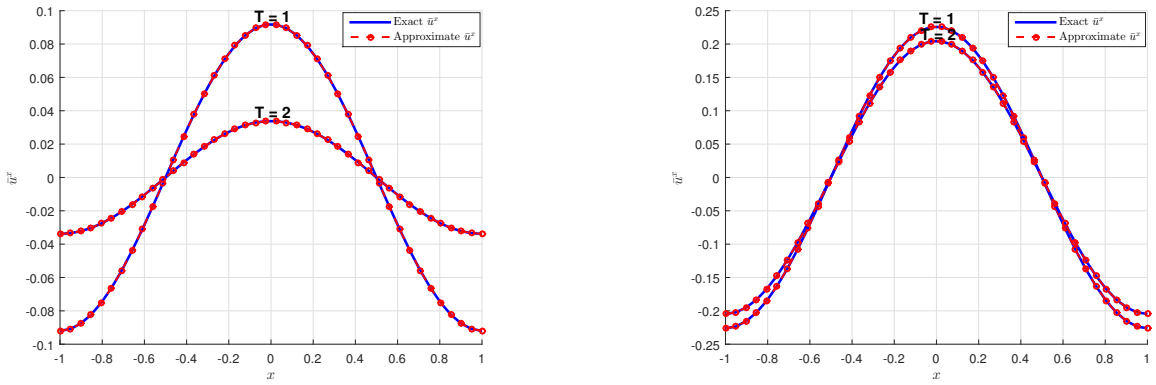

(a) Re=1, τ=0.025, a=0.025 **(b)** Re=10, τ=0.025, a=0.025

Figure 24: Comparison of numerical and exact solutions at different times using the present scheme

The proposed method performs well across a broad range of Reynolds numbers and typical time step sizes considered in this study. However, its behavior for very small time steps or highly stiff equations, particularly those involving sharp gradients or shock-like features, has yet to be thoroughly investigated. Such scenarios may lead to increased computational cost and potential stability challenges, which are common in numerical schemes for nonlinear partial differential equations. Addressing these limitations and enhancing the method's robustness under these conditions is planned for future work. Future efforts will focus on adaptive time stepping, implicit formulations, and stabilization techniques, as well as extensions to multidimensional

problems and complex geometries.

6 Conclusion

In this article, we introduced a scheme applied to the time-dependent Burgers' equation, which is a nonlinear convection-diffusion equation, with a number of *Re* equal to 100, 500, 1000, and 100000. In order to verify the applicability of this scheme, the numerical results were compared with the analytical solution, and it is found that the numerical results are in very good agreement with the analytical solutions, therefore the numerical scheme give quite good results, even for a large Reynolds number, and was motivated by its stability, convergence, and its precision. The current work opens several avenues for future research, including extending the scheme to two- and three-dimensional problems, application to the Navier–Stokes equations in cylindrical coordinates, and comparison with established methods such as FEM and FVM. These developments could make the proposed method suitable for complex simulations in fluid dynamics, turbulence modeling, and engineering applications involving realistic geometries.

References

Ahmed, N., Kumar, N., & Singh, S. (2021). Node averaged nodal integral method. In *14th WCCM-ECCOMAS Congress*, CIMNE.

Ahmed, N., Singh, S., and Kumar, N. (2024). Physics-based preconditioning of Jacobian-free Newton–Krylov solver for Navier–Stokes equations using nodal integral method. *International Journal for Numerical Methods in Fluids*, 96, 138–160.

Ahmed, N., Maurya, G., & Singh, S. (2023). A novel cell-centered nodal integral method for the convection-diffusion equation. *Annals of Nuclear Energy*, 189, 109858.

Ahmed, N., Singh, S. (2024). A modified cell-centered nodal integral scheme for the convection-diffusion equation. *Journal of Computational Science*, 80, 102320.

Ahmed N., Singh S., & Bharti R.P. (2025). Modified preconditioned Newton-Krylov approaches for Navier-Stokes equations using nodal integral method. *Computers & Mathematics with Applications* 181, 163–192.

Ahmed, N., Kompalli, U. S. S., & Singh, S. (2025). An improved cell-centered nodal integral approach for the transient diffusion equation. *Sādhanā*, 50, 1–12.

Ahmed, N., Bharti, R. P., & Singh, S. (2025). Efficient cell-centered nodal integral method for multi-dimensional Burgers' equations. *Engineering with Computers*.

Akhmouch, M., Guessous, N. (2003). High-order analytical nodal methods for the multi-group neutron diffusion equations. *Numerical Algorithms*, 34, 137–146.

Amrani, H.S., Akhmouch, M., & Guessous, N. (2006). Higher-order nodal integral method for the numerical solution of incompressible fluid flow equations. *Physical & Chemical News*, 30, 1–6.

Azmy, Y.Y. (1982). A Nodal Integral Method for the Numerical Solution of Incompressible Fluid Flow Problems. MS Thesis, University of Illinois.

Azmy, Y.Y. (1985). Nodal Method for Problems in Fluid Mechanics and Neutron Transport. University of Illinois at Urbana-Champaign.

Azmy, Y.Y., Dorning, J.J. (1983). A Nodal Integral Approach to the Numerical Solution of Partial Equations. In: *Advances in Reactor Computations*, American Nuclear Society, Vol. II, p. 893.

Burgers, J.M. (1939). Mathematical examples illustrating relations occurring in the theory of turbulent fluid motion.

Burns, T.J. (1979). The Partial Current Balance Method: A Nodal Green's Function Technique for Numerical Solution of Multidimensional Neutron Diffusion Problem. Ph.D. Thesis, University of Illinois.

Dorning, J. (1979). Modern Coarse-Mesh Methods: A Development of the 70s. In: *Computational Methods in Nuclear Engineering*, NTFIS, Washington, D.C., Vol. 1, pp. 31.

Fischer, H.D., Finnemann, H. (1981). The Nodal Integration Method — A Diverse Solver for Neutron Diffusion Problems. *Atomkerenergie, Kerntechnik*, 39(4).

Finnemann, H., Bennewitz, F. & Wagner, M.R. (1977). Interface Current Technique for Multidimensional Reactor Calculations. *Atomkerenergie*, 30.

Gander, M.J., Kumar, N. (2024). A new nodal integration method for Helmholtz problems based on domain decomposition techniques. *Domain Decomposition Methods in Science and Engineering XXVII*, 199–206.

Guessous, N. (1993). Méthodes nodales de discrétisation des équations de diffusion multigroupe. Ph.D. Thesis, Université Libre de Bruxelles.

Guessous, N. (2003). Higher-order analytical nodal methods for the discretization of diffusion equations. *Colloque Maghrébin TAM-TAM*, 14–18 Avril.

Hennart, J.P. (1986). A General Family of Nodal Schemes. *SIAM Journal on Scientific and Statistical Computing*, 7, 264.

Hennart, J.P. (1988). On the Numerical Analysis of Analytical Nodal Methods. *Numerical Methods for Partial Differential Equations*, 4, 233–254.

Jarrah I., Rizwan-Uddin. (2021). Nodal integral method for 3D time-dependent anisotropic convection-diffusion equation. *Ann. Nucl. Energy* 163, 108550.

Jarrah I., Rizwan-Uddin. (2022). Nodal integral methods in general 2D curvilinear coordinates – applied to convection–diffusion equation in domains discretized using quadrilateral elements. *Int. J. Heat Mass Transf.* 187, 122559.

Jarrah I., Rizwan-Uddin. (2024). Nodal integral method to solve the two-dimensional, time-dependent, incompressible Navier-Stokes equations in curvilinear coordinates. *Comput. Math. Appl.* 158, 219–243.

Kumar, N., Majumdar, R. & Singh, S. (2019a). Physics-based Preconditioning of Jacobian-Free Newton Krylov for Burgers' Equation Using Modified Nodal Integral Method. Department of Energy Science and Engineering, IIT Bombay, Mumbai, India.

Kumar, N., Majumdar, R. & Singh, S. (2019b). Predictor–Corrector Nodal Integral Method for Simulation of High Reynolds Number Fluid Flow Using Larger Time Steps in Burgers' Equation. Department of Energy Science and Engineering, IIT Bombay, Mumbai, India.

Kumar, N., Singh, S., & Doshi, J.B. (2013). Nodal integral method using quadrilateral elements for transport equations: part 1-convection-diffusion equation. *Numer. Heat Transf., Part B: Fundamen.* 64, 1–21.

Kumar, N., Singh, S., & Doshi, J.B. (2013). Nodal integral method using quadrilateral elements for transport equations: part 2-Navier-Stokes equations. *Numer. Heat Transf., Part B: Fundamen.* 64, 22–47.

Kumar, N., Shekar, B., & Singh, S. (2022). A nodal integral scheme for acoustic wavefield simulation. *Pure Appl. Geophys.,* 179, 3677–3691.

Lawrence, R.D. (1986). Progress in Nodal Methods for the Solution of the Neutron Diffusion and Transport Equations. *Progress in Nuclear Energy*, 17, 271–301.

Lawrence, R.D. (1979). A Nodal Green's Function Method for Multidimensional Neutron Diffusion Calculation. Ph.D. Thesis, University of Illinois.

Lawrence, R.D., Dorning, J.J. (1978). A Nodal Green's Function Method for Multidimensional Neutron Diffusion Calculation. *Trans. Am. Nucl. Soc.*, 28, 248.

Moussa, M.H.M., Abd Al-Halim, Z.M. (2022). Painlevé Analysis, Bäcklund Transformation and Exact Solutions for the (3+1)-Dimensional Nonlinear Partial Differential Equation Represented by Burgers' Equation. Department of Mathematics, Ain Shams University, Cairo, Egypt.

Raj, M., Ahmed, N., & Singh, S. (2022). Analytical nodal method for solution of neutron diffusion equation in polar coordinates. *Annals of Nuclear Energy*, 165, 108659.

Rizwan-uddin (1997). An Improved Coarse-Mesh Nodal Integral Method for Partial Differential Equations. *Numerical Methods for Partial Differential Equations*, 13, 113–147.

Shober, R.A., Sims, R.N., & Henry, A.F. (1977). Two nodal methods for solving time-dependent group diffusion equations. *Nuclear Science and Engineering*, 64, 582–592.

Steinke, R.G. (1973). A Coarse Nodal Method for Solving the Neutron Diffusion Equation. Ph.D. Thesis, University of Michigan.

Wang F., Rizwan-Uddin. (2003). A modified nodal scheme for the time-dependent, incompressible Navier-Stokes equations. *J. Comput. Phys.* 187 168–196.

Wang P., Rizwan-Uddin. (2018). A modified hybrid nodal-integral/finite-element method for 3D convection-diffusion problems in arbitrary geometries. *Int. J. Heat Mass Transf.* 122, 99–116.

Wang D., Li F., Guo J., Wei J., Zhang J., & Hao C. (2010). Improved nodal expansion method for solving neutron diffusion equation in cylindrical geometry. *Nucl. Eng. Des.* 240, 1997–2004.

Zhou X., Guo J., & Li F. (2016). General nodal expansion method for multi-dimensional steady and transient convection–diffusion equation. *Ann. Nucl. Energy* 88, 118–125.